GCM Simulations of Stable Isotopes in the Water Cycle in Comparison with GNIP Observations over East Asia

ZHANG Xinping[1*](章新平), SUN Zhian[2](孙治安), GUAN Huade[1,3](关华德), ZHANG Xinzhu[1](张新主), Wu Huawu[1](吴华武), and Huang Yimin[1](黄一民)

1 *College of Resources and Environmental Sciences, Hunan Normal University, Changsha* 410081, *China*

2 *Centre for Australian Weather and Climate Research, Melbourne* 3001, *Australia*

3 *School of the Environment, National Centre for Groundwater Research and Training, Flinders University, Adelaide* 5001, *Australia*

(Received April 5, 2011; in final form Septemper 21, 2011)

ABSTRACT

In this paper, we examine the performance of four isotope incorporated GCMs, i.e., ECHAM4 (University of Hamburg), HadCM3 (Hadley Centre), GISS E (Goddard Institute of Space Sciences), and MUGCM (Melbourne University), by comparing the model results with GNIP (Global Network of Isotopes in Precipitation) observations. The spatial distributions of mean annual δD and mean annual deuterium excess d in precipitation, and the relationship between δ^{18}O and δD in precipitation, are compared between GCMs and GNIP data over East Asia. Overall, the four GCMs reproduce major characteristics of δD in precipitation as observed by GNIP. Among the four models, the results of ECHAM4 and GISS E are more consistent with GNIP observed precipitation δD distribution. The simulated d distributions are less consistent with the GNIP results. This may indicate that kinetic fractionation processes are not appropriately represented in the isotopic schemes of GCMs. The GCM modeled MWL (meteoric water line) slopes are close to the GNIP derived MWL, but the simulated MWL intercepts are significantly overestimated. This supports that the four isotope incorporated GCMs may not represent the kinetic fractionation processes well. In term of LMWLs (local meteoric water lines), the simulated LMWL slopes are similar to those from GNIP observations, but slightly overestimated for most locations. Overall, ECHAM4 has better capability in simulating MWL and LMWLs, followed by GISS E. Some isotopic functions (especially those related to kinetic fractionation) and their parameterizations in GCMs may have caused the discrepancy between the simulated and GNIP observed results. Future work is recommended to improve isotopic function parameterization on the basis of the high-resolution isotope observations.

Key words: GCM, GNIP, stable isotope, deuterium excess, meteoric water line

Citation: Zhang Xinping, Sun Zhian, Guan Huade, et al., 2012: GCM simulations of stable isotopes in the water cycle in comparison with GNIP observations over East Asia. *Acta Meteor. Sinica*, **26**(4), 420–437, doi: 10.1007/s13351-012-0403-x.

1. Introduction

The water isotopes $H_2^{18}O$ and HDO are important environmental tracers for the water cycle, and useful climatic indicators. Firstly, on the global scale, stable isotopic compositions in precipitation change with mean surface temperature (Dansgaard, 1964; Merlivat and Jouzel, 1979; Aragúas et al., 1998). This relationship can be used to reconstruct palaeotemperatures where the historical water isotopic signatures are preserved. Secondly, the relationship between δ^{18}O and δD, shown in the meteoric water line (MWL) and deuterium excess d (=δD–8.0δ^{18}O), appears to be associated with the meteorological conditions of vapor resources for precipitation (Pfahl and Wernli, 2008, 2009; Uemura et al., 2008). Thirdly, the spatial and temporal variability of isotopic compositions in precipitation depends not only on temperature but also

Supported by the National Natural Science Foundation of China (40871094 and 41171035), Construct Program of the Key Discipline in Hunan Province (2011001), Open Fund of Key Laboratory of Tibetan Environment Changes and Land Surface Processes of the Chinese Academy of Sciences (2011004), Special Research Fund for the Doctoral Program of Higher Education (20094306110006), and Scientific Research Fund of Hunan Provincial Education Department (09A056).

*Corresponding author: zxp@hunnu.edu.cn.

on other atmospheric conditions such as the air mass origin and the intensity of precipitation (Dansgaard, 1964; Jouzel, 1986). These complex processes make climate reconstructions using precipitation isotopes more difficult. Nevertheless, if the effects of different processes are distinguished, precipitation isotopic signatures can be useful to infer more climatic information (Jouzel, 1986).

Almost at the same time as the GNIP (Global Network of Isotopes in Precipitation) sampling program was initiated, simple fractionation models have been developed to study the isotopic compositions of water vapor and precipitation as a function of atmospheric conditions (Dansgaard, 1964). These models took into account all the details of fractionation processes, but they only dealt with prescribed trajectories of isolated air masses. They have been successfully used to simulate observed mean temperature-isotope and δD–δ^{18}O relationships, and can also be used to study more complex dependencies, such as precipitation amount, air mass origin, and moving path (Dansgaard, 1964; Jouzel, 1986).

The only way to reconstruct complete spatial and temporal variations of stable isotopic compositions in vapor and in precipitation is to incorporate the stable isotope cycles into atmospheric general circulation models (GCMs). The GCMs explicitly simulate the global and regional features of atmospheric dynamics and thermodynamics and the detailed hydrological cycles. A GCM considers the complexity of dynamical and microphysical processes leading to the formation of individual precipitation event. It is also useful to examine the average observed climatic fields (e.g., on monthly timescale) which are the statistical results of successive precipitation events with highly variable characteristics (Joussaume et al., 1984; Jouzel et al., 1987; Hoffmann et al., 1998; Lee et al., 2007; Noone and Simmonds, 2002).

To facilitate the incorporation of stable water isotopes into the GCMs, the Global Energy and Water Cycle Experiment (GEWEX) has established the Stable Water Isotope Intercomparison Group (SWING) (http://www.bgc-jena.mpg.de/bgc-synthesis/projects/SWING/). SWING is to integrate the international efforts on the intercomparison of isotope-incorporated GCMs and the observation of stable water isotope in the atmosphere. Its aim is to understand the processes influencing stable isotope variations in the water cycle on different timescales, and to quantify their roles in climate feedback mechanisms (Vaughan, 2007).

To date, four GCMs, i.e., ECHAM4 (University of Hamburg) (Hoffmann et al., 1998), HadCM3 (Hadley Centre) (Tindall et al., 2009), GISS E (Goddard Institute of Space Sciences) (Schmidt et al., 2005, 2006), and MUGCM (Melbourne University) (Noone and Simmonds, 2002), have been involved in SWING. These models incorporate stable isotopic fractionation processes in the hydrological cycles. A 20-yr climatology control run has been performed with the four GCMs, using CO_2 concentrations at the level of 1980 and mean 1980–1999 sea surface temperatures from the HadISST 1 dataset (Hadley Centre Sea Ice and Sea Surface Temperature) (Rayner et al., 2003). The SWING S1B simulations run over 134 yr from 1870 to 2003 for ECHAM4 and MUGCM, to 2001 for HadCM3, and to 2000 for GISS E, with prescribed varying sea surface temperatures from the HadISST 1 dataset and representative atmospheric CO_2 concentrations for each year (Vaughan, 2007).

As an overall indication of the distribution of stable isotopes in global precipitation, average isotopes in precipitation are calculated from monthly model data from the SWING S1B experiment between the years 1961 and 2003 (2001 and 2000 for HadCM3 and GISS E models, respectively), which is coincident with the GNIP observation period. The geographic region of 10°–55°N, 75°–145°E is selected for comparison in this study. Inside this large East Asian region, the isotopic records at most GNIP stations, except Hong Kong and Bangkok, do not cover this entire period. For the single site survey, GNIP stations with more than 1 yr of continuous data have been selected to represent local climate variability. As this selection, there are 71 GNIP stations over East Asia (see Fig. 1). It can be seen that these selected stations are mainly located in eastern and southern Asia, but very rare in the northern and western parts of Asia, the Tibetan Plateau and its adjacent areas. In the past decades, many sampling stations have been set up in Northwest

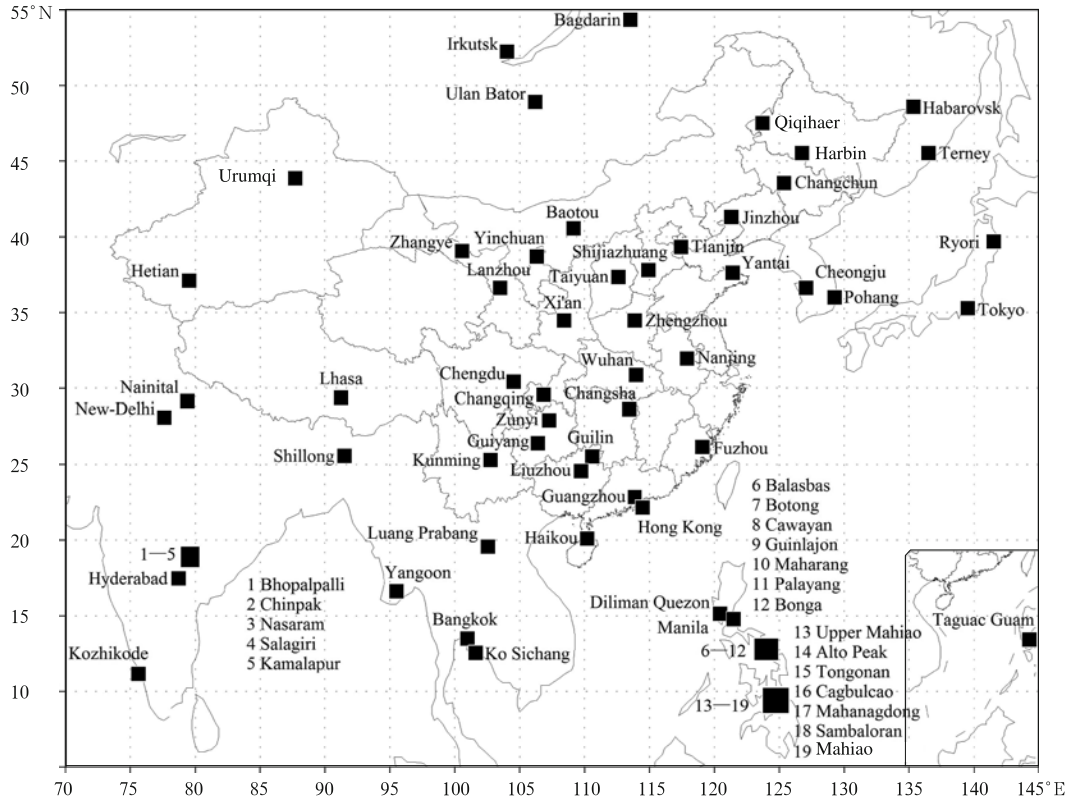

Fig. 1. GNIP sampling stations deployed by the IAEA/WMO over East Asia.

China and over the Tibetan Plateau (Tian et al., 2001; Liu et al., 2009) to understand the mechanism of the regional water cycle and atmospheric circulation patterns. Taking into account the systematic and continuous sampling, all selected sampling stations are from GNIP by the International Atomic Energy Agency/World Meteorological Organization (IAEA/WMO) in this study.

Using the SWING S1B data from the isotope enabled ECHAM4, GISS E, HadCM3, and MUGCM GCMs, and observed data from the selected GNIP stations, the spatial distribution of mean δD and the mean deuterium excess d in precipitation, and meteoric water line (MWL) are analyzed and compared, in order to assess modeling abilities of different isotope GCMs and to enhance the understanding of the energy and water cycle processes.

2. Model description

Stable water isotopes incorporated GCMs include $H_2^{18}O$ and HDO in every stage of the water cycle. The models simulate movement of water isotopes between the atmospheric grids and among the surface reservoirs following the same processes for H_2O (regular water). For the processes with phase changes, e.g., surface evaporation, atmospheric condensation, and re-evaporation of falling raindrops, isotopic fractionation is simulated. Both equilibrium and kinetic fractionations are considered. Although the hydrological processes along which no phase changes occur, such as surface runoff and vapor transport, do not cause isotope fractionation, they influence isotopic compositions of water reservoirs by mixing waters with different isotopic signatures. Thus, an appropriate transport scheme for advecting water and vapor of each isotopic composition between grid boxes is critical to simulating the observed isotopic fields (Joussaume et al., 1984; Jouzel et al., 1991).

In the implemented isotopic schemes, three processes involved in stable isotope fractionation are considered. Firstly, evaporation from ocean surface leads to isotopic fractionation, which is dependent on sea

surface temperature, specific humidity, and wind speed at the surface (Merlivat and Jouzel, 1979). Both equilibrium and kinetic fractionations are considered. Evapotranspiration from land surface is assumed to be transpiration dominant, and no isotopic fractionation is considered. Secondly, the condensation in water cloud is regarded as equilibrium fractionation. But kinetic fractionation is considered when vapor is condensed to ice. This is parameterized using a supersaturation function S_i, a simple linear function of the condensation temperature (Jouzel et al., 1987). In some situations, liquid water in super-cooled cloud can exist below freezing point (down to –40℃). In such cases, the isotopic equilibrium between liquid water and vapor is assumed. Thirdly, kinetic isotopic fractionation occurs when raindrops are falling into unsaturated air. In raindrops, isotopic equilibrium is maintained for large-scale liquid precipitation, but is only partially maintained for moist convective precipitation, since droplets there are assumed to be larger and fall faster (Jouzel, 1986).

2.1 ECHAM4

ECHAM GCM is a spectral atmosphere-ocean coupled model developed under the collaboration of the European Centre of Midium-Range Weather Forecasts in Reading and the Max-Planck Institut für Meteorologie in Hamburg. The fractionation effect of water isotopes is incorporated into the cycle of ECHAM version 4 model. The model can be run at the resolution of T42 which corresponds to the physical grid with a horizontal resolution of 2.8°×2.8° (time step of 24 min). The model includes 19 vertical levels in hybrid-sigma coordinates (Roeckner et al., 1996). The isotope hydrology developed for the ECHAM4 GCM is based on the scheme of Jouzel et al. (1987). This scheme was incorporated into an early version of the GISS GCM. Moisture movement was simulated with the semi-Lagrangian advection scheme of Rasch and Williamson (1990). In addition, ECHAM4 includes fractionation processes during the formation of cloud liquid water as well as a river runoff scheme as part of the surface hydrology (Hoffmann et al., 1998).

2.2 GISS E

GISS E is a Cartesian grid point model that can be run at a horizontal resolution of 8°×10°, or 4°×5°, or 2°×2.5°, and at either 20 or 23 vertical levels in sigma coordinates. A version of the NASA (National Aeronautics and Space Administration)/GISS GCM was the first model equipped with isotopic fractionation processes based on the pioneering work of Joussaume et al. (1984) with the GCM at the Laboratoire de Météorologie Dynamique (LMD). After that, isotopic processes have been incorporated into the GISS "Model E" GCM (Schmidt et al., 2005, 2006). When isotopic processes are simulated, the model is run at the relatively coarse 4°×5° horizontal resolution, and a quadratic upstream scheme is used for vapor advection. An important feature of GISS E is its capability to simulate complex cloud processes. This feature allows the use of stable water isotopes as diagnostic variables in various model sensitivity studies.

2.3 HadCM3

HadCM3 is an atmosphere-ocean coupled GCM developed by the Hadley Centre. It is composed of two main components, i.e., an atmospheric component (HadAM3) and an oceanic component (HadOM3). Both components can either be coupled together or run separately. The atmospheric part of HadCM3 is a hydrostatic grid point model using the Arakawa B grid and hybrid-sigma vertical coordinates. The horizontal resolution is 3.75°×2.5°, and there are 19 vertical levels. The simulation time step is 30 min. The model uses a conservative split-explicit integration scheme with fourth-order horizontal advection as described by Cullen and Davies (1991); with this, the advection of water vapor and its isotopes depend upon their respective spatial gradients.

2.4 MUGCM

MUGCM (Melbourne University GCM) is a spectral primitive equation model of the atmosphere based on Bourke et al. (1977) and McAvaney et al. (1978). MUGCM has been used extensively for climate studies, numerical weather prediction studies, and development of new physical parameterizations. For this study, MUGCM is configured to have a horizontal resolution denoted by the rhomboidal truncation of the harmonic series at wavenumber 21 (R21). To allow quadratic products to be calculated on the transform

grid with perfect accuracy, the 3.25°×5.625° grid points are required. In the vertical direction, there are 9 discrete levels in hybrid-sigma coordinates. The MUGCM isotopic schemes are based on those implemented in ECHAM4 (Lee et al., 2007), and it uses a semi-Lagrangian moisture transport scheme similar to that used in ECHAM4. In addition, MUGCM allows water isotopic ratios varying on the ocean surface. It also includes isotopic formulae for snow and stream runoff processes (Brown, 2003).

3. Simulation results

3.1 Spatial distribution of mean precipitation

The distribution and intensity of precipitation can be reliably simulated by a model capable of accurately portraying the distribution of isotopes in precipitation. Of all the processes simulated by modern atmospheric GCMs, the processes of convection and precipitation are still poorly represented, and this becomes a significant source of errors (Gates et al., 1999). A useful dataset to validate modeled precipitation is the NCEP Climate Prediction Center Merged Analysis of Precipitation (CMAP) analysis with a horizontal resolution of 3.75°×2.5° for the period 1979–2007. CMAP is derived from gauge observations, infrared and passive microwave satellite data, and assimilated data from the NCEP-NCAR reanalysis (Xie and Arkin, 1997). This dataset can be used as a general indicator of the spatial distribution and intensity of global precipitation. However, the data are less reliable in the regions of sparse data and poleward of 60° in both the Northern and Southern Hemispheres. For this study on the low-mid latitude range, it provides a good basis (Fig. 2a) to examine the performance of selected GCMs. However, it should be noted that the CMAP dataset only covers 25 yr of the 43-yr simulation period.

On annual timescale, there are precipitation maxima over the equator and the tropical western Pacific associated with warm sea surface temperatures and the seasonal movement of the intertropical convergence zone (ITCZ). The precipitation maxima are also recorded over the northern Bay of Bengal due to the onset of the Indian monsoon. Meanwhile, precipitation minima appear over the large areas from Mongolia to western China, and weak precipitation shows up over the subtropical western Pacific. Additionally, dramatic variations of precipitation are observed along the northwest edge of the East Asian monsoon region, where marine and continental air masses interact frequently.

The GCM simulated distributions of annual precipitation averaged over 1961–2003 are shown in Figs. 2b–2d. In comparison to the CMAP distribution, all four GCMs capture the basic features of the precipitation distribution. The zonal distribution is well simulated by ECHAM4 and HadCM3 while it is ambiguous in GISS E and MUGCM simulations. For the precipitation maxima over the India-Burma regions, different GCMs produce different positions and intensities. For example, the precipitation maxima lie in the northeast of this region from GISS E, but in its south from HadCM3. ECHAM4 simulations do not catch such a region distinctly, and MUGCM simulations give an opposite result, i.e., there appears a precipitation minimum. These differences in simulated precipitation will eventually affect the simulation of stable isotopic composition in precipitation.

3.2 Spatial distribution of mean δD

In the study region, 71 GNIP stations having more than 1 yr of continuous sampling records are selected to compare with the GCM results. The reported monthly δD in precipitation at the 71 GNIP stations is averaged to obtain mean annual δD in precipitation (Fig. 3a). Despite of different sample sizes at these stations, Fig. 3a shows that: (1) the precipitation δD in low latitudes is greater than that in high latitudes; (2) δD over oceans is greater than that over continents, especially the inland areas; and (3) δD in high altitudes is lower than that in low altitudes. It is found that the information on stable isotopic spatial changes provided by actual survey is limited and without enough details. This is unfavorable to the restoration of paleoclimate records needed in the investigation of water resources using stable isotope methodology. However, by recurring to the numerical analyses of isotope GCM results under the prerequisite of the

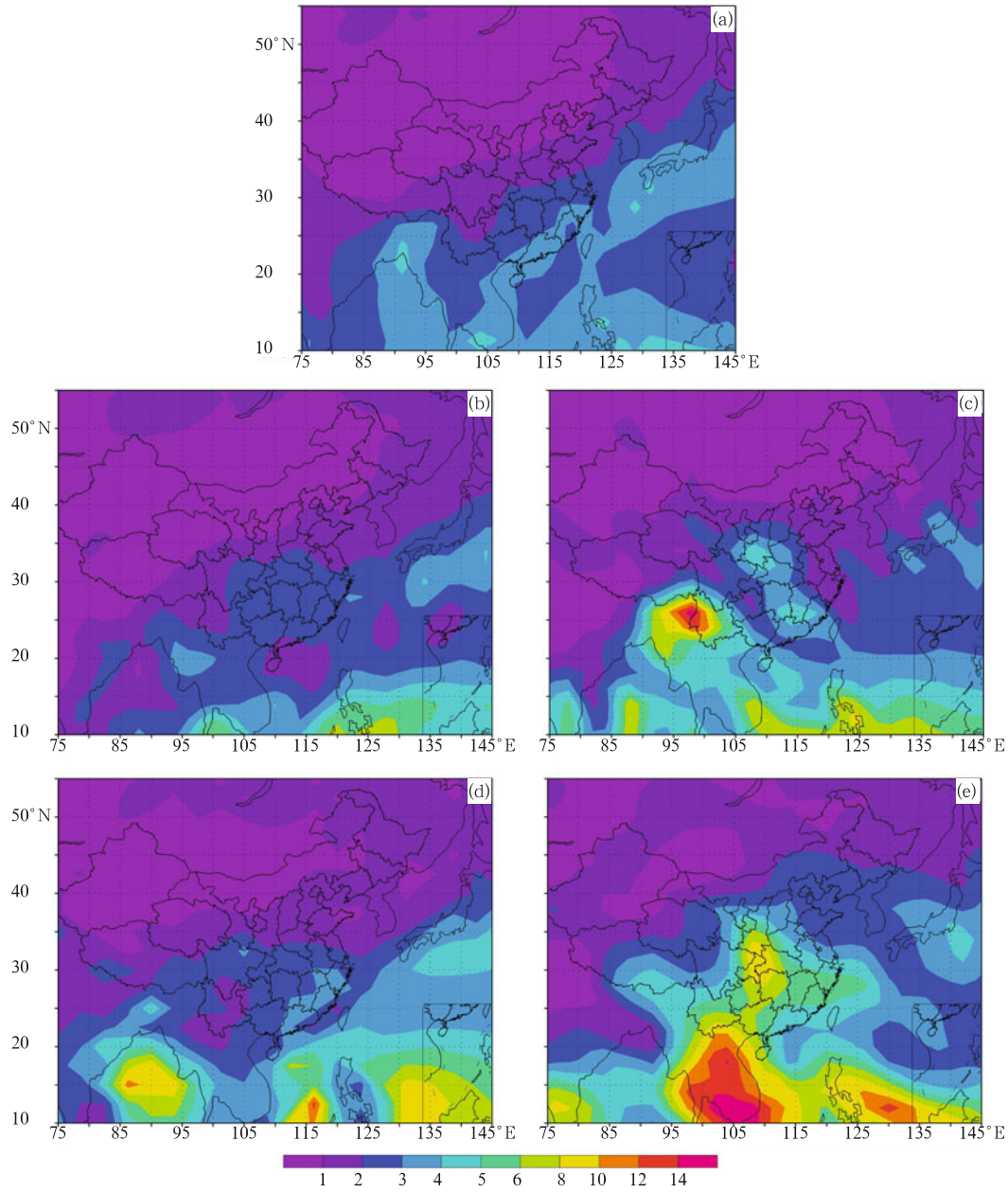

Fig. 2. Distributions of mean annual precipitation (mm day^{-1}) over East Asia. (a) Calaculated by CMAP dataset for the period 1979–2003, and simulated by (b) ECHAM4, (c) GISS E, (d) HadCM3, and (e) MUGCM for the period 1961–2003.

simulated changes matching the actual observations, the situation can be radically improved.

Figures 3b–3e show the spatial distributions of the mean annual δD in precipitation over East Asia for 1961–2003, simulated by ECHAM4, GISS E, HadCM3, and MUGCM, respectively. The spatial distributions of simulated precipitation δD by four GCMs are in good agreement with the GNIP observations, and they provide more refined information. The observed precipitation δD distribution features are decently captured in the model results.

The simulation results reveal that precipitation δD distribution reflects the effects of geographical background of different air masses and the interaction between them. In low latitudes, the precipitation isotopes are generally enriched. The maximal δD in pre-

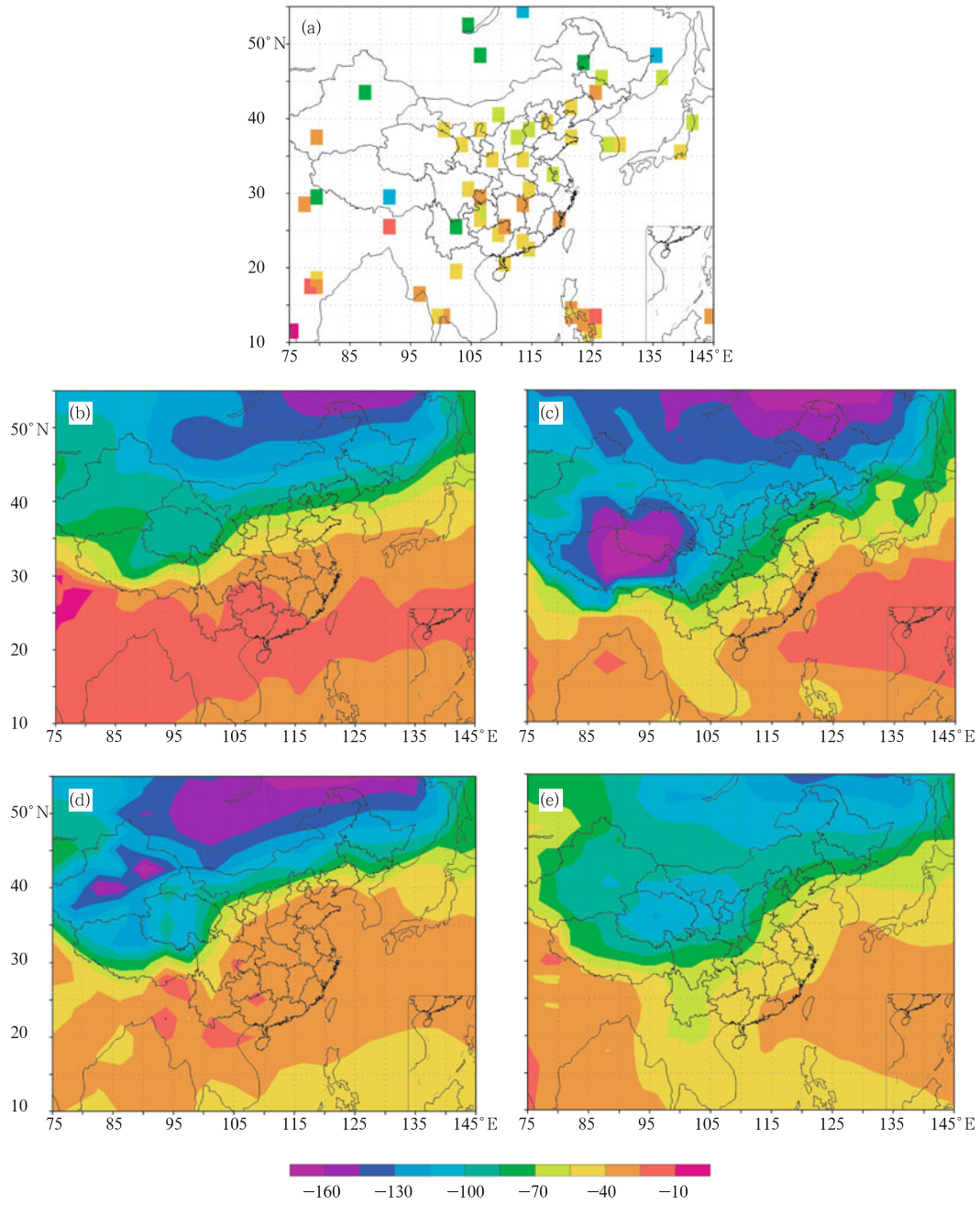

Fig. 3. Comparison of the mean annual δD in precipitation for 1961–2003. (a) Surveyed at 71 GNIP stations and simulated by (b) ECHAM4, (c) GISS E, (d) HadCM3, and (e) MUGCM.

cipitation appears either over the western Pacific that is controlled by the subtropical high (e.g., GISS E and MUGCM simulations), or in the inland areas of central South Peninsula (e.g., ECHAM4 simulation). Along the east coast of the mainland, the precipitation δD decreases toward inland, and displays northeast-southwest oriented isolines. This region has the most steep δD gradient, probably resulted from frequent marine and continental air masses interactions.

The first minimal precipitation δD occurs in the northeastern part of the study area, where the mean temperature is low due to high latitude. The second

minimal δD appears over the Tibetan Plateau and its surrounding areas where the temperature is low due to high altitude. For the second δD minimum, different GCM simulations give different isotopic ranges, locations, and intensities. In the ECHAM4 simulation, the low-value areas over the Tibetan Plateau seem to be a southwestward extension of the first minimum over the Siberia. The second minimum is somewhat captured by HadCM3 and MUGCM, but the center location of this minimum lies to the northwest of the plateau in HadCM3 while it is to the northeast in MUGCM. The GISS E simulation shows a large second minimum, which agrees with the sparse observations in this area, indicating possible impact of the Tibetan Plateau on precipitation isotopes.

Vapor isotopic distributions are not so well documented as precipitation δD distributions. The simulated annual mean vapor δD between 1000 and 500 hPa is shown in Fig. 4. The δD distribution shows a zonal pattern, with vapor δD greater in low latitudes than that in high latitudes. All four GCM results consistently show a vapor δD minimum in East Siberia, which is in agreement with the precipitation δD minimum. This vapor δD minimum from the MUGCM simulation covers a much larger area than that from the other three model simulations. Of the four GCMs, only GISS E gives a vapor δD minimum over the Tibetan Plateau, corresponding to the simulated second precipitation δD minimum. Overall, the simulated vapor δD in the low-mid atmosphere shows similar spatial distribution patterns to the simulated precipitation δD. This indicates that precipitation isotopic signatures are primarily controlled by the source vapor isotope compositions.

To further examine the performance of GCMs, co-located simulated precipitation δD and GNIP observed value are plotted in Fig. 5. The regressions of the simulated with the observed values are performed,

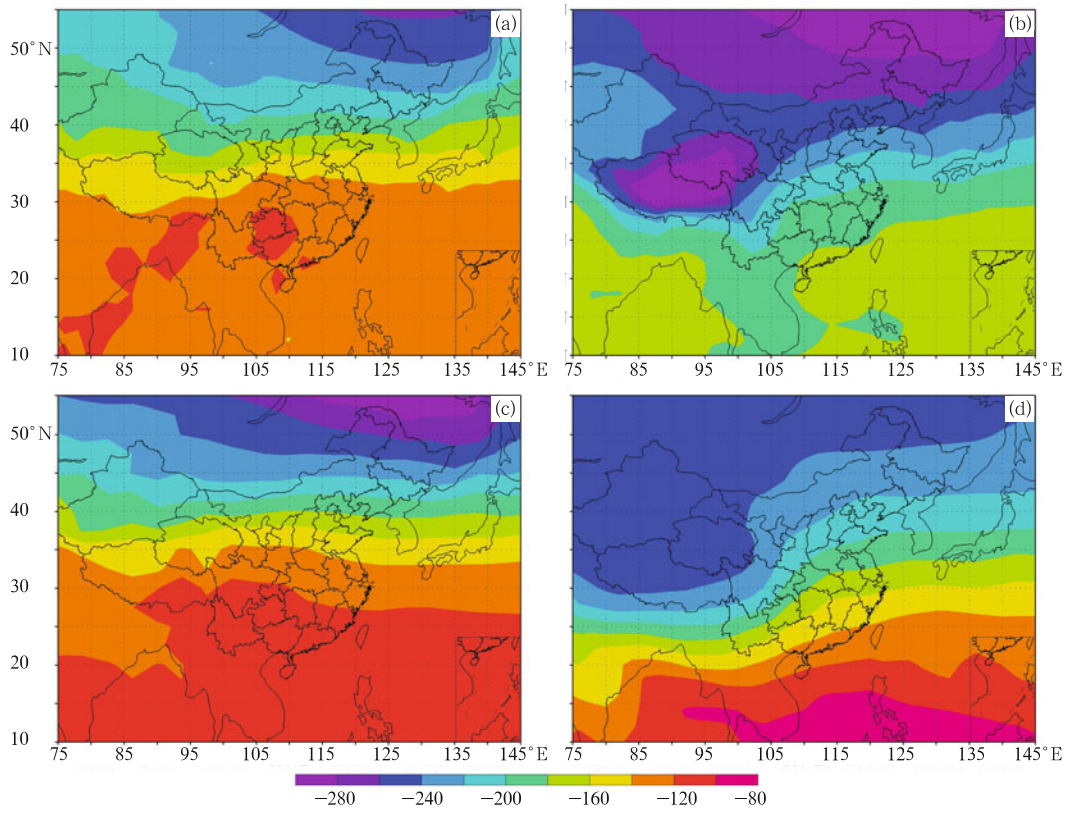

Fig. 4. Distributions of Simulated mean δD in vapor between 1000 and 500 hPa. (a) ECHAM4, (b) GISS E, (c) HadCM3, and (d) MUGCM.

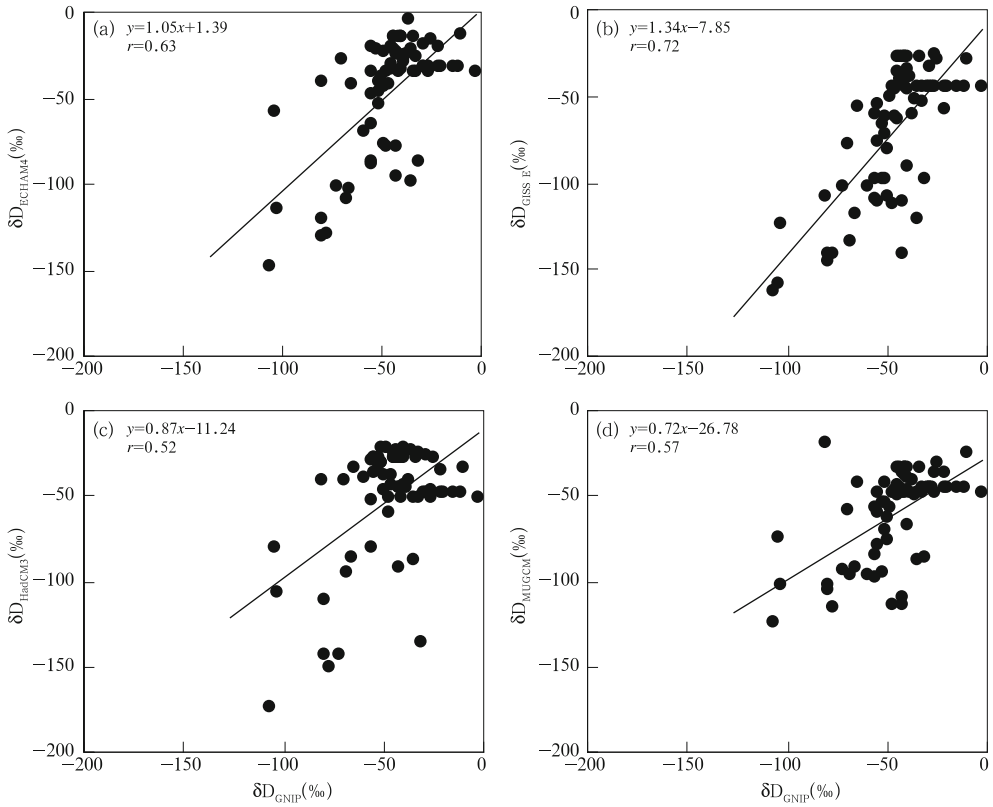

Fig. 5. Comparison between the mean annual δD in precipitation calculated at GNIP stations and simulated by (a) ECHAM4, (b) GISS E, (c) HadCM3, and (d) MUGCM at corresponding grid boxes over East Asia.

with results summarized in the following,

$$\begin{aligned} &y = 1.05x + 1.39 \\ &\quad (\text{ECHAM4}; r = 0.63, \sigma_y/\sigma_x = 1.66, n = 71), \\ &y = 1.34x - 7.85 \\ &\quad (\text{GISS E}; r = 0.72, \sigma_y/\sigma_x = 1.86, n = 71), \\ &y = 0.87x - 11.24 \\ &\quad (\text{HadCM3}; r = 0.52, \sigma_y/\sigma_x = 1.66, n = 71), \\ &y = 0.72x - 26.78 \\ &\quad (\text{MUGCM}; r = 0.57, \sigma_y/\sigma_x = 1.27, n = 71), \end{aligned} \quad (1)$$

where x is GNIP precipitation δD, and y is the modeled δD at corresponding grid boxes.

The mean δD ranges from –2.4‰ at Alto Peak (11.1°N, 124.74°E; 796 m) to –106.5‰ at Bagdarin (54.47°N, 113.58°E; 903 m) in GNIP observations, but from –4.92‰ at New Delhi (28.58°N, 77.2°E; 212 m) (actual value of –36.7‰) to –147.89‰ at Bagdarin by ECHAM4, from –26.12‰ at Guam (13.55°N, 144.83°E; 110 m) (actual value of –26.7‰) to –162.76‰ at Bagdarin by GISS E, from –21.46‰ at Chengdu (30.67°N, 104.02°E; 506 m) (actual value of –39.3‰) to –174.37‰ at Bagdarin by HadCM3, and from –19.47‰ at Nainital (29.4°N, 79.46°E; 1953 m) (actual value of –80.6‰) to –124.75‰ at Bagdarin by MUGCM. All modeled minimal δD in precipitation is located at Bagdarin, while the modeled maximal δD is at different stations.

It can be seen that the four standard deviation values of mean annual δD simulated by the four GCMs are all greater than the observations, showing that the simulated mean δD has relatively large spatial variability. The regression results suggest that ECHAM4 and GISS E perform better than the other two in terms of capturing the observed spatial distribution of the mean annual δD in precipitation.

3.3 Spatial distribution of mean deuterium excess

The deuterium excess d ($= \delta\text{D} – 8\delta^{18}\text{O}$) is a second-

order parameter derived from δD and δ^{18}O. The variation of d is mainly resulted from kinetic fractionation processes in the water cycle. First, preferential evaporation of light isotopes such as D makes d in evaporated vapor increase during ocean surface evaporation. As the evaporation process is closely associated with temperature, relative humidity, and wind speed in vapor origins, d in evaporated vapor is governed by meteorological conditions. Second, as heavy isotopes such as ^{18}O condense easily, the d value in initial condensates is reduced relatively to vapor during vapor condensation, but at the same time, the d value in residual vapor is increased. With the continuance of condensation process in cloud, the rate D/H becomes successively heavier relative to the rate ^{18}O/^{16}O in residual vapor. Therefore, d in residual vapor will increase constantly in the absence of external vapor, and d in condensates as the derivative of vapor will also increase constantly. Third, when raindrops fall in unsaturated atmosphere, the kinetic fractionation process happens, and thus d in falling raindrops and in precipitation will be decreased. Fourth, the re-evaporation process over the land surface will increase the vapor d and the resulted precipitation d eventually (Zhang et al., 2009). Impacted by the factors mentioned above, precipitation d in some regions may lose the function as the tracer of meteorological conditions in vapor origins. But in any case, through analyzing precipitation d, one can track macroscopically the complex meteorological processes of vapor from origins to precipitation sites, and reveal quantitatively the impact of different mechanisms on vapor d and precipitation d.

The spatial distribution of observed mean precipitation d is shown in Fig. 6a. The maximal precipitation d of 15.0‰ appears at Bayan station (13.06°N, 123.93°E; 520 m) and nearby in the Philippines. At Guilin (25.07°N, 110.08°E; 170 m) and Guiyang (26.58°N, 106.72°E; 1071 m), precipitation d reaches 14.8‰ and 14.4‰, respectively. The appearance of high d in precipitation is probably related to the initial condensation of vapor and supplement of vegetation transpiration with high d. The minimal precipitation d of 2.0‰ appears at Changchun station (43.06°N, 123.93°E; 520 m). At Bagdarin and Ulanbator (47.93°N, 106.98°E; 1338 m), precipitation d is 2.7‰ and 3.0‰, respectively. The low d values over inland areas are probably related to the evaporation of falling raindrops in unsaturated atmosphere, while the low d at Changchun and its surrounding regions is probably a result of a low d in source vapor. At Urumqi (43.78°N, 87.62°E; 918 m) and Hetian (37.13°N, 79.93°E; 1375 m), which are also located in drought regions, higher precipitation d of 12.5‰ and 11.1‰ are seen. This is owing to a high d moisture source, likely from inland surface evaporation.

The GCM simulated annual mean precipitation d distributions are shown in Figs. 6b–6e. In comparison with the modeled δD, the simulated d distributions are far less consistent with the GNIP results. This may indicate that kinetic fractionation processes are not appropriated represented in the isotopic schemes of GCMs.

It can be seen that the spatial distribution of d in precipitation is characterized by a latitudinal distribution. The precipitation d, basically less than 10‰, is relatively low over the low-latitude oceans. The lowest precipitation d over the Indian Peninsula and the subtropical western Pacific in ECHAM4 and MUGCM simulations is related to falling raindrop evaporation. In HadCM3, the minimal d over north-central Xinjiang is inconsistent with observation. This is probably because the HadCM3 model overestimates the impact of the evaporation of falling raindrops on reducing d in precipitation in this region.

The simulated maximum precipitation d of more than 18‰, from all four GCMs, occurs over the Tibetan Plateau and its surrounding areas, especially over the southern plateau. No GNIP data are available to validate this simulated precipitation d pattern. Nevertheless, measurements by Tian et al. (2005) show that precipitation d can reach up to 17.5‰ in central Himalayas and 10‰–30‰ at Nyalam before the summer monsoon onset. This suggests that the GCM simulated maximum d over the Tibetan Plateau

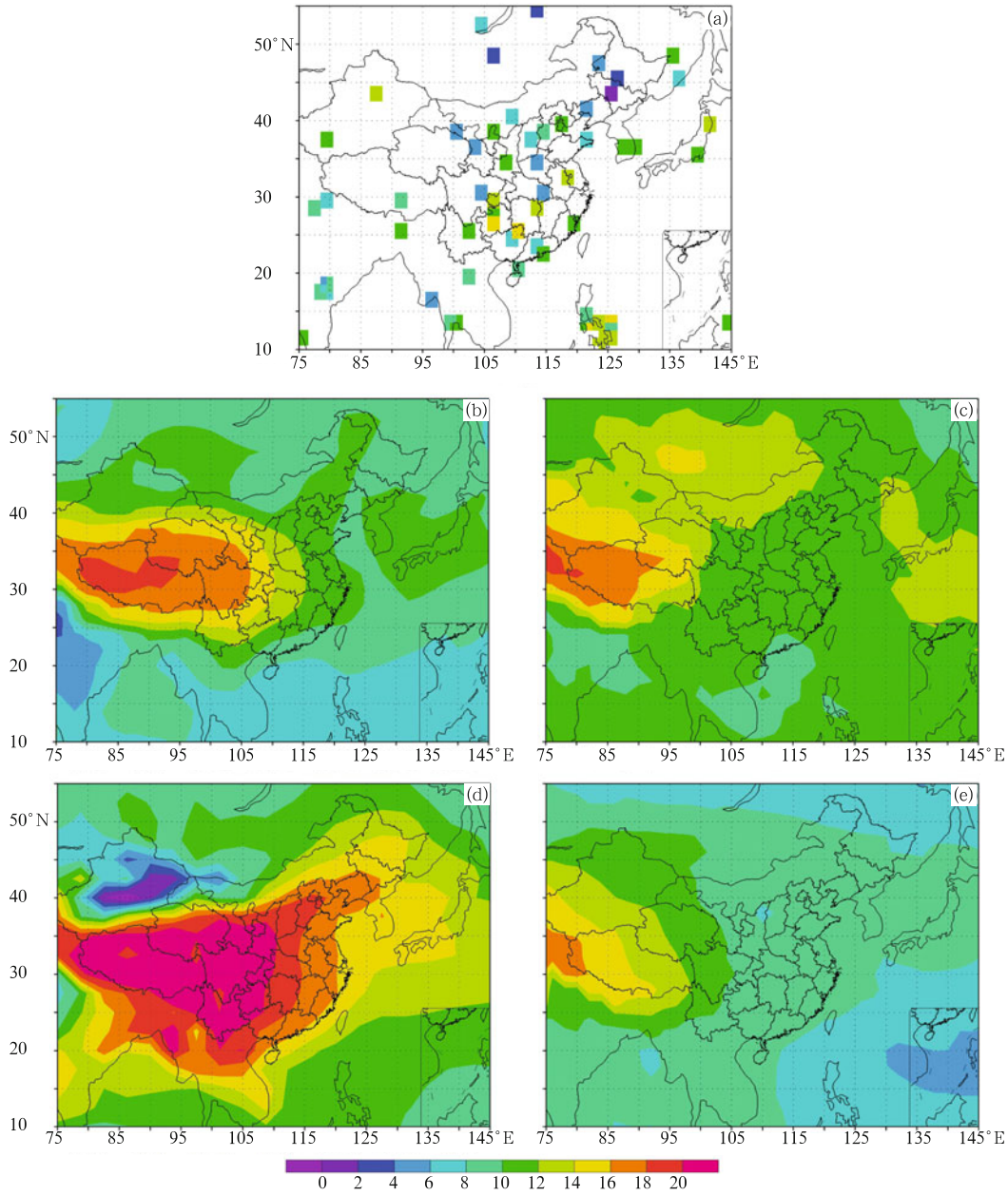

Fig. 6. Comparison of the mean annual deuterium excess in precipitation in 1961–2003. (a) Surveyed at 71 GNIP stations and simulated by (b) ECHAM4, (c) GISS E, (d) HadCM3, and (e) MUGCM.

may reflect the actual precipitation d in this area.

The simulated high precipitation d over the Tibetan Plateau is apparently associated with the high d value in the vapor source over this area (Fig. 7). Models ECHAM4, GISS E, and HadCM3 all show high d in vapor over the Tibetan Plateau. Physically, two mechanisms could lead to a large vapor d. One is the local moisture recycling, the other is the constant rainout of vapor over the long-distance moisture transport.

The high d in vapor between 1000 and 500 hPa that appears over East Siberia in the ECHAM4, EISS E, and HadCM3 simulations does not result in high d in precipitation over this region. This may be related to the impact of the evaporation of falling raindrops. The distribution of mean d in precipitation over this region is consistent with that of the mean d in vapor

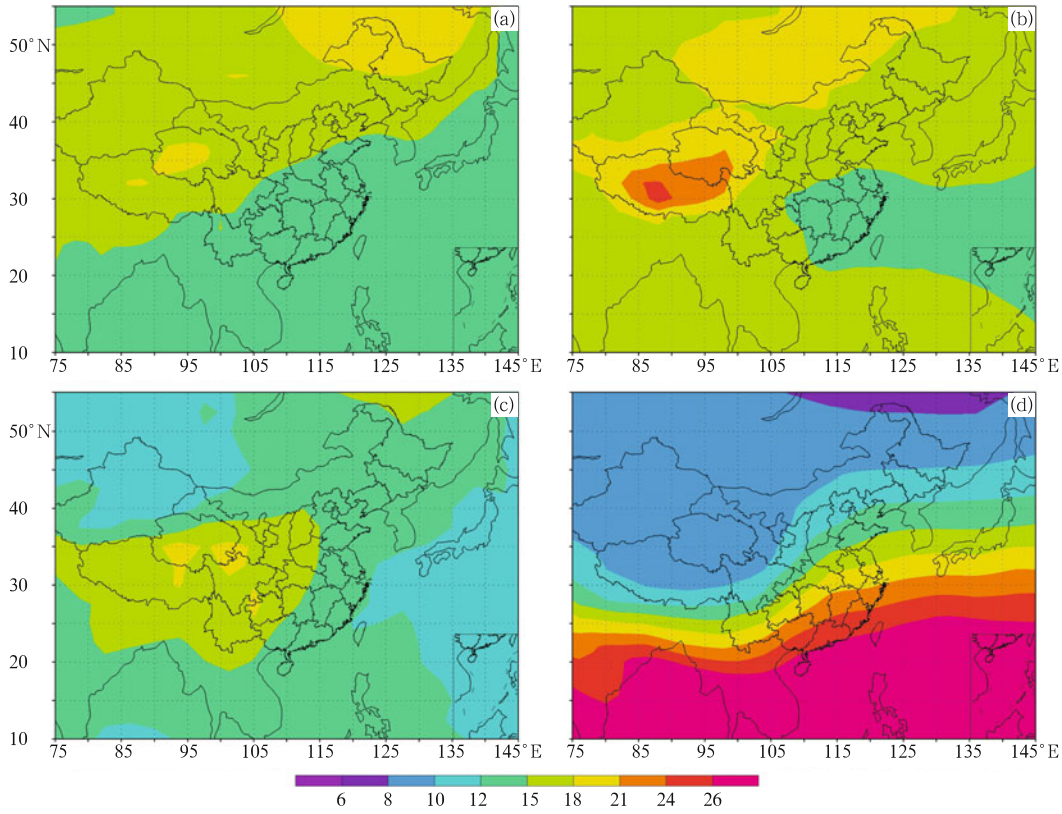

Fig. 7. Distributions of Simulated mean deuterium excess in vapor between 1000 and 500 hPa. (a) ECHAM4, (b) GISS E, (c) HadCM3, and (d) MUGCM.

between 850 and 700 hPa (figure omitted), indicating that precipitation may come from the condensation in this layer.

The MUGCM simulation has completely different vapor d distribution patterns from the other three models. Further work is needed to examine the differences among the models, in particular between MUGCM and the other three.

3.4 Simulations and comparisons of MWL

The meteoric water line (MWL), defined by Craig (1961), describes the relative abundance of the two isotopes in precipitation:

$$\delta D = 8.0\delta^{18}O + 10.0‰. \quad (2)$$

The MWL of a specific region is slightly different from GMWL (global meteoric water line). The slope of MWL is mainly governed by the $[\alpha(\mathrm{D})-1]/[\alpha(^{18}\mathrm{O})-1]$ ratio (α is the equilibrium fractionation coefficient), and reflects the difference of equilibrium fractionation between H_2O and HDO, and between H_2O and $H_2{}^{18}O$. The intercept of MWL, reflecting the deviation degree of deuterium from the equilibrium state, essentially results from the kinetic isotopic effect that occurs when water evaporates from ocean surface.

The MWL in Fig. 8a is calculated by the observed mean annual δD and δ^{18}O at selected 71 GNIP stations over East Asia as

$$\delta\mathrm{D} = 7.63\delta^{18}\mathrm{O} - 0.04‰. \quad (3)$$

The MWL reveals the relationship between δD and δ^{18}O in precipitation over East Asia. Its slope being slightly lower than 8.0 refects the impact of the nonequilibrium fractionation in the water cycle, which is supported by an MWL intercept far smaller than 10.0‰.

The GCM simulated precipitation isotopic distributions are sampled at the grids of the 71 GNIP stations to calculate MWLs (Figs. 8b–8e):

$\delta D = 7.74\delta^{18}\mathrm{O} + 8.13‰$ (ECHAM4),

$$\delta D = 7.84\delta^{18}\mathrm{O} + 9.31‰ \text{ (GISS E)},$$
$$\delta D = 8.42\delta^{18}\mathrm{O} + 18.29‰ \text{ (HadCM3)},$$
$$\delta D = 8.00\delta^{18}\mathrm{O} + 8.86‰ \text{ (MUGCM)}. \quad (4)$$

These simulated MWLs show a consistent linear relationship between δD and δ^{18}O in precipitation with the correlation coefficient of more than 0.99. The simulated MWL slopes, except for the HadCM3 simulation, are close to the observation. Especially in the ECHAM4 simulation, the difference between the two is only 0.11. If the differences in sample size and spatial resolution between GCM simulations and the GNIP observations are considered, the slight difference in MWL slopes calculated from GCM results and GNIP observations are reasonable. However, all simulated MWL intercepts are significantly larger than that from GNIP observations. This discrepancy suggests that all four GCMs fail to simulate some processes influencing deuterium excess, consistent with our previous analysis. As for the HadCM3 simulation, the larger MWL slope and intercept compared with those of the GNIP observations is probably associated with the inappropriate high supersaturation function at ice surface in mixed clouds.

In the above, MWLs derived from mean annual precipitation isotopic compositions over the space are examined. In order to examine GCM simulated local meteoric water line (LMWL), 11 GNIP stations with the longest observation records over East Asia are selected. Lhasa station (29.70°N, 91.13°E; 3649 m) with only 7-yr observations is also selected because of its special location. Table 1 gives the LMWLs calculated by monthly stable isotopic ratios in precipitation at the 12 selected GNIP stations and simulated by the four GCMs at 12 corresponding grid boxes, respectively.

Among the 12 GNIP stations, the maximal slope and intercept of LMWL, both of which occurr at Guilin, are 8.38 and 16.76‰; while the minimal ones, both at Shijiazhuang (38.03°N, 114.42°E; 80 m), are

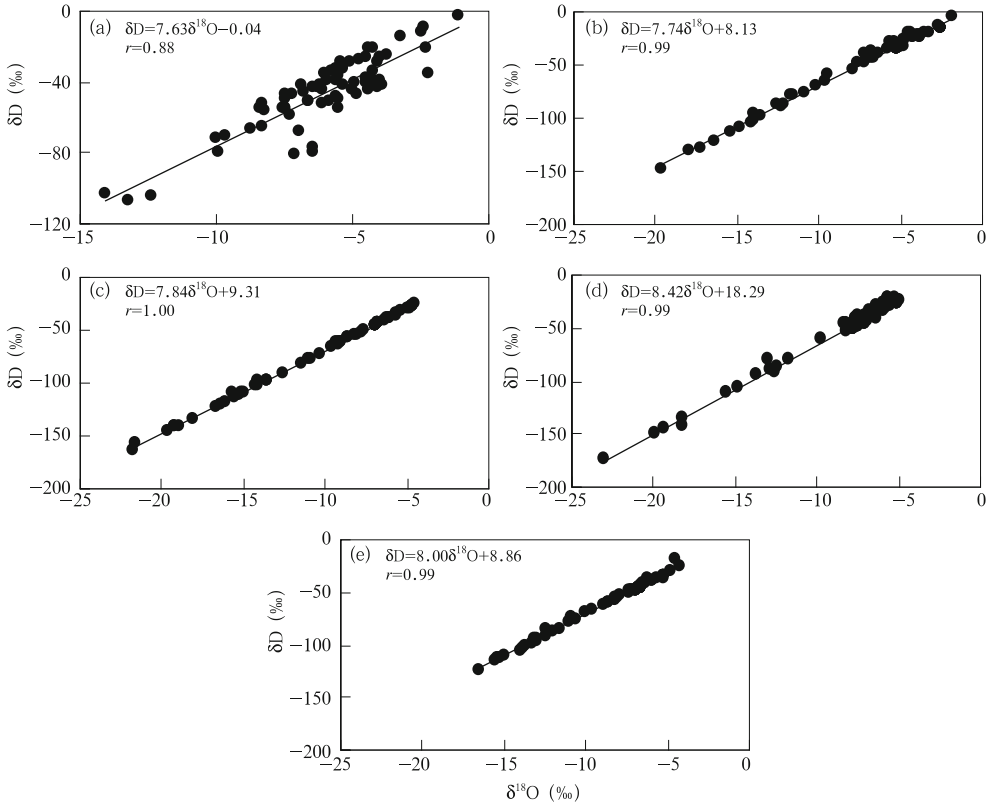

Fig. 8. Meteoric water lines (a) calculated by observations at 71 GNIP stations and simulated by (b) ECHAM4, (c) GISS E, (d) HadCM3, and (e) MUGCM at corresponding grid boxes over East Asia.

6.07 and –5.76‰, respectively; at Hong Kong (22.32°N, 114.17°E; 66 m), Pohang (36.03°N, 129.38°E; 6 m), and Lhasa stations, the LMWL slops are all close to 8.0, and the intercepts are all greater than 10.0‰; at the other 8 stations, LMWL slopes are significantly lower than 8.0, while the intercepts are smaller than 10.0‰, showing the impact of non-equilibrium evaporation process.

It has been well documented that LMWLs vary with sea surface conditions of the moisture source area, atmospheric circulation patterns, and local weather conditions (Dansgaard, 1964; Merlivat and Jouzel, 1979). LMWL of precipitation in the moisture origin area of high temperature and high humidity will have a lower slope than that in the moisture origin area of low temperature and low humidity (Zhang et al., 2005). LMWL of precipitation from advection has a lower slope than that from convection (Zhang et al., 2003). Supersaturation in cloud leads to a bigger slope in the resulted precipitation LMWL (Zhang et al., 2003). Evaporation of falling raindrops will result in a smaller LMWL slope (Zhang et al., 2003). Thus, the slope of LMWL is generally bigger in low latitudes than in high latitudes, as well as in humid regions than in drought regions. As shown in Table 1, these trends exist but not significantly, indicating that single hydrometeorological factor cannot fully explain the variability of LMWL slopes. In addition, even at the stations with basically similar LMWL, their climate characteristics can be quite different. For example, the LMWL slope at Urumqi (6.98) is almost the same as that at Guam (7.01). The low LMWL slope in the former is primarily caused by dry climate, but that in the latter is associated with local high temperature and high humidity (Zhang et al., 2005). In the East Asian monsoon region, the difference in LMWL is attributed to different vapor sources between winter and summer monsoons. Usually, precipitation that originates from warm and humid ocean and with high unstable energy, strong convection, and weak evaporation under cloud base has a relatively large LMWL slope, while precipitation that originates from recycled

Table 1. Comparison between LMWL calculated by observations at 11 GNIP stations with the longest survey records plus Lhasa station and simulated by ECHAM4, GISS E, HadCM3, and MUGCM at corresponding grid boxes over East Asia

Station	GNIP	ECHAM4	GISS E	HadCM3	MUGCM
Bangkok	δD=7.56δ^{18}O+6.68	δD=7.73δ^{18}O+6.01	δD=8.46δ^{18}O+13.52	δD=8.50δ^{18}O+14.38	δD=7.71δ^{18}O+7.20
	P=1499 mm, n=315	P=1670 mm, n=516	P=1968 mm, n=480	P=1649 mm, n=492	P=5532 mm, n=516
Guam	δD=7.01δ^{18}O+6.10	δD=7.98δ^{18}O+6.62	δD=7.90δ^{18}O+10.14	δD=8.10δ^{18}O+10.12	δD=7.31δ^{18}O+2.37
	P=2659 mm, n=106	P=2699 mm, n=516	P=2352 mm, n=480	P=3292 mm, n=492	P=2192 mm, n=516
Guilin	δD=8.38δ^{18}O+16.76	δD=8.70δ^{18}O+15.53	δD=7.92δ^{18}O+9.75	δD=9.33δ^{18}O+26.80	δD=8.62δ^{18}O+14.19
	P=1531 mm, n=91	P=1286 mm n=516	P=1697 mm, n=480	P=1522 mm, n=492	P=3552 mm, n=516
Hongkong	δD=8.02δ^{18}O+10.55	δD=8.57δ^{18}O+10.66	δD=7.65δ^{18}O+8.07	δD=9.26δ^{18}O+23.81	δD=8.42δ^{18}O+10.88
	P=2279 mm, n=379	P=1033 mm, n=516	P=1577 mm, n=480	P=1689 mm, n=492	P=1906 mm, n=516
Kunming	δD=6.56δ^{18}O–2.96	δD=8.53δ^{18}O+17.93	δD=8.11δ^{18}O+12.01	δD=9.23δ^{18}O+29.36	δD=8.64δ^{18}O+15.83
	P=991 mm, n=151	P=1026 mm, n=516	P=3146 mm, n=480	P=1173 mm, n=492	P=2911 mm, n=516
Lhasa	δD=8.08δ^{18}O+12.37	δD=7.96δ^{18}O+17.65	δD=8.20δ^{18}O+19.30	δD=9.51δ^{18}O+41.75	δD=8.80δ^{18}O+22.25
	P=424 mm, n=42	P=549 mm, n=516	P=763 mm, n=480	P=853 mm, n=492	P=2281 mm, n=51
New Delhi	δD=7.17δ^{18}O+4.39	δD=7.74δ^{18}O+9.02	δD=8.01δ^{18}O+11.92	δD=7.97δ^{18}O+9.97	δD=8.29δ^{18}O+13.27
	P=784 mm, n=290	P=351 mm, n=516	P=162 mm, n=480	P=721 mm, n=492	P=116 mm, n=516
Pohang	δD=8.08δ^{18}O+12.92	δD=7.22δ^{18}O+5.50	δD=8.28δ^{18}O+14.31	δD=9.23δ^{18}O+22.37	δD=8.31δ^{18}O+10.91
	P=1106 mm, n=110	P=1036 mm, n=516	P=1295 mm, n=480	P=1064 mm, n=492	P=1352 mm, n=516
Ryori	δD=7.54δ^{18}O+9.33	δD=7.07δ^{18}O+3.55	δD=8.03δ^{18}O+11.43	δD=9.37δ^{18}O+23.19	δD=7.88δ^{18}O+7.56
	P=1385 mm, n=183	P=1171 mm, n=516	P=887 mm, n=480	P=1239 mm, n=492	P=1145 mm, n=516
Shijiazhuang	δD=6.07δ^{18}O-5.76	δD=7.46δ^{18}O+6.30	δD=7.69δ^{18}O+7.19	δD=9.36δ^{18}O+26.11	δD=8.10δ^{18}O+9.39
	P=538 mm, n=146	P=657 mm, n=516	P=936 mm, n=480	P=674 mm, n=492	P=1714 mm, n=516
Tokyo	δD=6.87δ^{18}O+4.70	δD=7.58δ^{18}O+8.45	δD=8.65δ^{18}O+18.08	δD=9.78δ^{18}O+25.71	δD=7.64δ^{18}O+6.57
	P=1378 mm, n=183	P=1407 mm, n=516	P=2167 mm, n=480	P=1945 mm, n=492	P=2164 mm, n=516
Urumqi	δD=6.98δ^{18}O+0.43	δD=7.48δ^{18}O+2.57	δD=7.88δ^{18}O+10.15	δD=8.11δ^{18}O+5.43	δD=8.17δ^{18}O+13.58
	P=306 mm, n=131	P=231 mm, n=516	P=69 mm, n=480	P=19 mm, n=492	P=884 mm, n=516

The correlation coefficients are all greater than 0.93 in column GNIP and greater than 0.99 in GCM simulations.

vapor in inland areas and with strong advection and evaporation under cloud base has a relatively small LMWL slope.

For the GCM simulated LMWLs at the 12 GNIP stations collocated grids, the slopes and intercepts range from 7.07 to 8.70 and 2.57‰ to 17.93‰ for ECHAM4, from 7.65 to 8.65 and 7.19‰ to 19.30‰ for GISS E, from 7.97 to 9.78 and 5.43‰ to 41.75‰ for HadCM3, and from 7.31 to 8.80 and 2.37‰ to 22.25‰ for MUGCM, respectively. In comparison, ECHAM4 performs the best to capture LMWLs at the 12 selected stations, followed by GISS E. Overall, the simulated LMWL slopes are similar to those from GNIP observations, but slightly overestimated for most locations. Especially, in the HadCM3 and MUGCM simulations, LMWL slopes at all 12 stations are overestimated. Several factors may have contributed to the overestimation: (1) the coverage and length of available data. At these selected 12 stations, Hongkong and Lhasa have the longest and shortest survey records of 379 and 42 months, respectively, but the GCM grid box has comparatively complete and continuous data; (2) the details in the water cycle and resolution of model. As is known, GNIP data represent the situation at a single station, but model data represent the average in the grid box; (3) the simulation of precipitation. The deviations of simulated precipitation from observation affect isotopic simulations in precipitation to some degree, especially in the regions with marked amount effect; and (4) the assumption of the supersaturation function at ice surface S_i. For HadCM3, the supersaturation function is $S_i = 1.0–0.005T$ (T is the cloud temperature in degrees Celsius), but for the other three models, the function is $S_i = 10–0.004T$. An overestimated S_i may lead to overestimated dynamic effect, and result in synchronous increases of the slope and intercept of MWL, because light isotopes such as D have a faster fractionation rate than heavy isotopes such as ^{18}O during kinetic fractionation. This artifact is evident in the HadCM3 simulation.

4. Conclusions and discussion

Stable water isotopes provide a good tool for investigation of water resources, diagnosis of atmospheric circulation patterns, and restoration of paleoclimate. The GNIP data provide useful information that benefits the study of global and regional water cycle and paleoclimate. However, GNIP and other field sampling methods often suffer drawbacks such as sparse sampling network, short sample duration, long sample accumulation time, etc. In this regard, modeling approaches, such as GCM, compensate these shortcomings. In this paper, we examine the performance of four selected isotope incorporated GCMs, i.e., ECHAM4, GISS E, HadCM3, and MUGCM by comparing the model results with GNIP observations. The spatial distribution of mean annual δD and mean annual deuterium excess d in precipitation, and the relationship between δ^{18}O and δD in precipitation, are compared between GCM simulations and GNIP data over East Asia.

Overall, the four GCMs reproduce major characteristics of stable isotopes in precipitation as observed by GNIP, for example, latitude effect, continent effect, and altitude effect. In low latitudes, precipitation is generally enriched in heavy isotopes. The models also capture the high gradient in precipitation δD along the east coast of East Asia that results from strong interactions of marine and continental air masses. The two minimal precipitation δDs are reproduced by the GCMs as well. One such minimum, corresponding to the lowest mean temperature, appears in the northeastern parts of East Asia. The other minimal δD, corresponding to the highest altitude, appears over the Tibetan Plateau and its surrounding areas. Among the four models, the results of ECHAM4 and GISS E are more consistent with the GNIP observed precipitation δD distribution.

Compared with δD, the simulated d distributions are less consistent with the GNIP data. This indicates that kinetic fractionation processes are not appropriately represented in the isotopic schemes of GCMs. Nonetheless, all four models show that a maximal precipitation d occurs over the Tibetan Plateau and its surrounding areas, especially over the southern plateau, which may represent the actual physical condition in the areas.

The GCM modeled MWL slopes are close to the GNIP derived MWL, but the simulated MWL intercepts are significantly overestimated. This further supports that the four isotope incorporated GCMs cannot well represent the kinetic fractionation processes. In terms of LMWLs, the simulated LMWL slopes are similar to those from GNIP observations, but slightly overestimated for most locations. Overall, ECHAM4 has better capability in simulating MWL and LMWL, followed by GISS E.

Although isotope enabled GCMs can reproduce spatial and temporal variations of stable precipitation isotopic compositions, and reveal the relationship and interaction between stable water isotopes in the water cycle and their impact factors, there are still some inconsistencies between simulated and observed results. For example, compared with actual survey, δD in mid-high latitude inland areas is systematically underestimated by all the four GCMs. This is related to the isotopic scheme used in the GCMs. In those isotopically underestimated regions, the formation of rainfall is usually affected by large scale advection, and thus stable isotopic fractionation in cloud is assumed to be in equilibrium. The hydrometeor is immediately removed from cloud system after its formation under the assumption. This will inevitably result in the acceleration of stable isotopic fractionation and finally lead to reduction of stable isotopes in precipitation (Dansgaard, 1964). In addition, some assumptions involving isotopic fractionation are also not accurate enough in isotope GCMs. For example, parameterization process of kinetic fractionation in convective clouds is expressed using a supersaturation function at ice surface (only a linear function of temperature). We suggest to use high-resolution isotope surveys and eliminate gradually the dependence of hydrological simulations on empirical formulations.

It can be seen from Fig. 3a that there appear same stable isotopic values around the middle Yellow River and the Pearl River basins, even though both regions have very different climatic background and circulation conditions (Su et al., 2003; Xue et al., 2007). However, all the four models do not reproduce such a distribution feature. The inconsistencies between regional simulations and observations on a longer timescale may be attributed to the differences in the detail of vapor processes and model resolution. Simulated results represent the average situation of a grid box rather than a single point value.

The intercomparisons of different GCM simulations show some discrepancies among the models as well. For example, the vapor d distribution patterns between 1000 and 500 hPa simulated by MUGCM are very different from those of the other three models. Because the isotopic schemes used and the initial forcing are basically similar in the GCMs, the discrepancies among these simulations are related to the internal structure, resolution, and vapor transport scheme in each model. There is less detail about that in this study. Nevertheless, isotope enabled GCM is undoubtedly the most important tool to reproduce spatial and temporal variations of stable water isotopes and to unscramble subtly the relationship and interaction between stable isotopes and atmospheric factors in the water cycle.

Acknowledgments. We thank the Stable Water Isotope Intercomparison Group (SWING) and Dr. Julia Tindall for providing the GCM modeling stable water isotopes, and also thank the IAEA/WMO for providing the GNIP data over Asia.

REFERENCES

Aragúas-Aragúas, L., K. Froehlich, and K. Rozanski, 1998: Stable isotope composition of precipitation over Southeast Asia. *J. Geophys. Res.*, **103**, 28721–28742.

Dansgaard, W., 1964: Stable isotopes in precipitation. *Tellus*, **16**(4), 436–468.

Bourke, W., B. McAvaney, K. Puri, et al., 1977: Global modeling of atmospheric flow by spectral methods. *Methods in Computational Physics*. Chang, J., Ed., Academic Press, **17**, 267–324.

Brown, J., 2003: The response of stable water isotopes in precipitation and the surface ocean to tropical climate variability. Ph.D. thesis, University of Melbourne, Melbourne, 254 pp.

Craig, H., 1961: Isotopic variations with meteoric water. *Science*, **133**, 1702–1703.

Cullen, M., and T. Davies, 1991: A conservative split-explicit integration scheme with 4th-order horizontal advection. *Quart. J. Roy. Meteor. Soc.*, **117**, 993–1002.

Gates, W. L., J. S. Boyle, C. Covey, et al., 1999: An overview of the results of the Atmospheric Models Intercomparison Project. *Bull. Amer. Meteor. Soc.*, **80**, 29–55.

Hoffmann, G., M. Werner, and M. Heimann, 1998: Water isotope module of the ECHAM atmospheric general circulation model: A study on timescales from days to several years. *J. Geophys. Res.*, **103**, 16871–16896.

Joussaume, S., R. Sadourny, and J. Jouzel, 1984: A general circulation model of water isotope cycles in the atmosphere. *Nature*, **311**, 24–29.

Jouzel, J., 1986: Isotopes in cloud physics: Multiphase and multistage condensation processes. *Handbook of Environmental Isotope Geochemistry.* Elsevier Sci. Pub. Amsterdam, **2**, 61–112.

——, G. L. Russell, and R. J. Suozzo, 1987: Simulations of the HDO and $H_2^{18}O$ atmospheric cycles using the NASA-GISS General Circulation Model–The seasonal cycle for present day conditions. *J. Geophys. Res.*, **92**, 14739–14760.

——, R. D. Koster, R. J. Suozzo, et al., 1991: Simulations of the HDO and $H_2^{18}O$ atmospheric cycles using the NASA GISS GCM: Sensitivity experiments for present-day conditions. *J. Geophys. Res.*, **94**, 7495–7507.

Lee, J. E., I. Fung, D. J. DePaolo, et al., 2007: Analysis of the global distribution of water isotopes using the NCAR atmospheric general circulation model. *J. Geophys. Res.*, **112**, doi: 10.1029/2006JD007657.

Liu Zhongfang, Tian Lide, Yao Tandong, et al., 2009: Spatial distribution of $\delta^{18}O$ in precipitation over China. *Chinese Sci. Bull.*, **54**(6), 804–811.

McAvaney, B. J., W. Bourke, and K. Puri, 1978: A global spectral model for simulation of the general circulation. *J. Atmos. Sci.*, **35**, 1557–1583.

Merlivat, L., and J. Jouzel, 1979: Global climatic interpretation of the deuterium–^{18}O relationship for precipitation. *J. Geophys. Res.*, **84**, 5029–5033.

Noone, D. C., and I. Simmonds, 2002: Associations between $\delta^{18}O$ of water and climate parameters in a simulation of atmospheric circulation for 1979–1995. *J. Climate*, **15**, 3150–3169.

Pfahl, S., and H. Wernli, 2008: Air parcel trajectory analysis of stable isotopes in water vapor in the eastern Mediterranean. *J. Geophys. Res.*, **113**, doi: 10.1029/2008JD009839.

——, and ——, 2009: Lagrangian simulations of stable isotopes in water vapor: An evaluation of nonequilibrium fractionation in the Craig-Gordon model. *J. Geophys. Res.*, **114**, doi: 10.1029/2009JD012054.

Rasch, P. J., and D. L. Williamson, 1990: Computational assessment of moisture transport in global models of the atmosphere. *Quart. J. Roy. Meteor. Soc.*, **116**, 1071–1090.

Rayner, N. A., D. E. Parker, E. B. Horton, et al., 2003: Global analyses of sea surface temperature, sea ice, and night marine air temperature since the late nineteenth century. *J. Geophys. Res.*, **108**, doi: 10.1029/2002JD002670.

Roeckner, E., J. M. Oberhuber, A. Bacher, et al., 1996: ENSO variability and atmospheric response in a global coupled atmosphere-ocean GCM. *Climate Dyn.*, **12**, 737–754.

Schmidt, G. A., G. Hoffmann, D. T. Shindell, et al., 2005: Modeling atmospheric stable water isotopes and the potential for constraining cloud processes and stratosphere-troposphere water exchange. *J. Geophys. Res.*, **110**, doi: 10.1029/2005JD005790.

——, R. Ruedy, J. E. Hansen, et al., 2006: Present day atmospheric simulations using the GISS Model E: Comparison to in-situ, satellite and reanalysis data. *J. Climate*, **19**, 153–192.

Su Xiaosi, Lin Xueyu, Liao Zisheng, et al., 2003: Variation of isotopes in the Yellow River along the flow path and its affecting factors. *Geochimica*, **32**(4), 349–357. (in Chinese)

Tian Lide, Yao Tandong, Sun Weizhen, et al., 2001: Relationship between δD and $\delta^{18}O$ in precipitation on north and south of the Tibetan Plateau and moisture recycling. *Sci. China (Series D)*, **44**(9), 789–796.

——, ——, J. W. C. White, et al., 2005: Westerly moisture transport to the middle of Himalayas revealed from the high deuterium excess. *Chinese Sci. Bull.*, **50**(10), 1026–1030.

Tindall, J. C., P. J. Valdes, and L. C. Sime, 2009: Stable water isotopes in HadCM3: Isotopic signature of El Niño-Southern Oscillation and the tropical amount effect. *J. Geophys. Res.*, **114**, doi: 10.1029/2008JD010825.

Uemura, R., Y. Matsu, K. Yoshimura, et al., 2008: Evidence of deuterium excess in water vapor as an indicator of ocean surface conditions. *J. Geophys. Res.*, **113**, doi: 10.1029/2008JD010209.

Vaughan, J. I., 2007: An evaluation of observed and simulated high-resolution records of stable isotopes in precipitation. Ph.D. thesis, University of Melbourne, Melbourne, 268 pp.

Xie, P., and P. A. Arkin, 1997: Global precipitation: A 17-year monthly analysis based on gauge observations, satellite estimates, and numerical model outputs. *Bull. Amer. Meteor. Soc.*, **78**, 2539–2558.

Xue Jibin, Zhong Wei, and Zhao Yinjuan, 2007: Variations of δ^{18}O in precipitation in the Zhujiang (Pearl) River and its relationship with ENSO event. *Scientia Geographica Sinica*, **27**(6), 825–830. (in Chinese)

Zhang Xinping, Yao Tandong, Liu Jingmiao, et al., 2003: Simulations of stable isotopic fractionation in mixed cloud in middle latitudes—taking the precipitation at Urumqi as an example. *Adv. Atmos. Sci.*, **20**(2), 261–268.

——, Tian Lide, and Liu Jingmiao, 2005: Fractionation mechanism of stable isotope in evaporating water body. *J. Geograph. Sci.*, **15**(3), 375–384.

——, Yang Zongliang, Niu Guoyue, et al., 2009: Stable water isotope simulation in different reservoirs of Manaus, Brazil, by Community Land Model incorporating stable isotopic effect. *Int. J. Climatol,*, **29**(5), 619–628.